Article

Modelling Tree Growth in Monospecific Forests from Forest Inventory Data

Guadalupe Sáez-Cano [1,*] , Marcos Marvá [1] , Paloma Ruiz-Benito [2] and Miguel A. Zavala [3]

[1] Forest Ecology and Restoration Group, Departamento de Física y Matemáticas, Facultad de Ciencias, Universidad de Alcalá, 28805 Madrid, Spain; marcos.marva@uah.es
[2] Forest Ecology and Restoration Group, Departamento de Ciencias de la Vida, Facultad de Ciencias, Universidad de Alcalá, 28805 Madrid, Spain; paloma.ruizb@uah.es
[3] Forest Ecology and Restoration Group, Edificio Ciencias, Campus Universitario, Universidad de Alcalá, 28805 Alcalá de Henares, Spain; ma.zavala@uah.es
*   Correspondence: lupe.saez@uah.es

Abstract: The prediction of tree growth is key to further understand the carbon sink role of forests and the short-term forest capacity on climate change mitigation. In this work, we used large-scale data available from three consecutive forest inventories in a Euro-Mediterranean region and the Bertalanffy–Chapman–Richards equation to model up to a decade's tree size variation in monospecific forests in the growing stages. We showed that a tree-level fitting with ordinary differential equations can be used to forecast tree diameter growth across time and space as function of environmental characteristics and initial size. This modelling approximation was applied at different aggregation levels to monospecific regions with forest inventories to predict trends in aboveground tree biomass stocks. Furthermore, we showed that this model accurately forecasts tree growth temporal dynamics as a function of size and environmental conditions. Further research to provide longer term prediction forest stock dynamics in a wide variety of forests should model regeneration and mortality processes and biotic interactions.

Keywords: carbon storage; differential equations; National Forest Inventory; dbh dynamics; short-term prediction

1. Introduction

Forests play a key role in the carbon balance worldwide and harbour more than 2/3 of terrestrial biodiversity [1–3]. Global forest biomass is increasing worldwide [4] and forest growth is the main process in European forests for biomass increases during the last few decades [3,5]. The role of forests in climate regulation is being increasingly recognized by the scientific community and international policies, particularly since the Kyoto Protocol in 1997. Therefore, land use, land-use change, and forestry (LULUCF) activities are aiming to further increase the carbon stored in tree biomass, where forest management within forests is critical to maintain, monitor, and predict the role of forests in climate mitigation.

Forests have the potential to provide a key and complementary role in both absorbing atmospheric carbon dioxide and conserving biodiversity (e.g., [6,7]). Proper accounting and prospective scenarios of carbon storage by forests are particularly needed in order to implement specific actions and accomplish mitigation targets.

Forest biomass and carbon storage monitoring rely on different data sources that target different levels and scales of biological organization [8,9]. Targeting the tree and the stand level allows us to obtain accurate estimates of above-ground biomass over decadal and regional scales when systematic forest inventories are available. Specifically, tree and stand growth dynamic models allow us to project forest growth over time so forest stocks can be estimated over a rotation period. Roughly, the idea consists in stating a growth law

that fits well the actual stand structure and uses it to make stand variables change over time as a function of key drivers such as environmental conditions or competition.

Tree growth is driven by several factors, chiefly size, resource availability, and environmental conditions [10,11]. Process-based models explicitly describe carbon assimilation and stomatal responses to resource and environmental variation [12]. In contrast, empirical tree growth models describe these effects by explicitly describing resource variability—e.g., light and soil water availability [13,14]—or through density-dependence effects [15] or a combination of these effects [10,16].

There is a wide range of dynamical models, from individual-scale to landscape models, that can be used to support forest management and policy [8,9]. As data availability of forest responses to climate change is increasing worldwide, particularly in Europe [17], it is increasing the range of forest models being applied at regional and global scales for a wide variety of purposes [18,19]. Yet, parameterization and validation of forest stock models from local to regional scales require the availability of systematic and observational data [19]. National forest inventories, and particularly those that are open-access, provide the opportunity to estimate the short- to mid-term (up to decades) changes in above-ground basal areas [20,21] and the mitigation potential of existing forests and tree plantation efforts, particularly from local to regional levels and for above-ground tree-level biomass.

Ordinary differential equations (ODE) are a flexible approximation to describe tree-level growth dynamics when repeated temporal observations are available. An ODE relates the rate of change of a variable of interest (for instance, diameter at breast height, DBH) to the current state of such a variable (current DBH). The solution of such an ODE is a function DBH(t) that provides the values DBH on time, so that one can project DBH on time. ODEs are empirical models [22] used to predict community dynamics [23,24]. Among the main advantages of ODEs are their predictive, extrapolative ability [24].

The well-known Bertalanffy–Chapman–Richards (BCR) ordinary differential equation [25–27] has been widely used to model DBH growth in time: it is biologically interpretable, versatile, and easy to be parameterized. However, it is key to determine how many temporal censuses are required in order to obtain an adequate parameterization. Although the explicit solution of this equation has been used for this purpose both worldwide [28] and in Spanish forests [29], alone or within the so-called generalized algebraic difference approach [30], we showed that, using the BCR ordinary differential equation, three censuses are an adequate approximation for modelling short-term forest stocks' dynamics. This allowed us to exploit large-scale National Forest Inventory (NFI) data for prospective mitigation analyses. In this work, we assessed the robustness of this model by using monospecific plots in three consecutive inventories (Spanish National Forest Inventory) occupied by the four dominant species in the Barcelona region (Catalonia, Spain), and we explored whether the BCR equation is a reliable tool to assess regional tree growth dynamics from forest inventory observations. In particular, our objectives were: (i) to test this equation as an individual distance-independent individual-tree growth model using minimal (length three) time series data; (ii) to examine the role of intraspecific competition; (iii) to validate the model in plots with one single initial observation; and, (iv) to scale-up this method to the stand or the forest level by assembling individual trees.

2. Materials and Methods

We used the tree DBH-level data obtained from three Spanish NFIs [31,32] as well as geographical climate (temperature and rainfall) information [33]. We considered the species *Pinus sylvestris* (Psy), *Pinus halepensis* (Pha), *Pinus nigra* (Pni), and *Quercus ilex* (Qil), the most abundant species in the province of Barcelona (Catalonia, Spain). We selected monospecific plots (i.e., at least 80% of the basal area of the plot was of the target species).

2.1. National Forest Inventory Database

We used available Spanish NFI data from the second, third, and fourth inventories (1986–1990, 1999–2005, and 2010–current, for the NFI2, NFI3, and NFI4, respectively). In

the NFI2, a systematic network of plots each in km^2 over forested areas was established [31] and re-measured in the NFI3 [34] and NFI4 [32]. Each NFI plot had a variable radius design, comprised of four concentric circular subplots of 5, 10, 15, and 25 m where adult trees less than 12.5 cm, less than 22.5 cm, less than 42.5 cm, and larger or equal to 42.5 cm were measured, respectively. For each sampled tree, its height, DBH, species identity, distance to the center of the plot, and the position of the tree (i.e., centesimal degrees from the North) were recorded.

To parameterize growth relationships, we considered only individuals present from NFI2 to NFI4 as at least 3 DBH records were needed in order to fit the equations. However, the reduction in tree number in the NFI database was nearly negligible (less than 4% in the 10-year interval between consecutive NFIs) [29]. Thus, for each tree, we had a temporal series of DBH of length three, considering only trees with positive DBH growth. We selected monospecific plots of the target species in Barcelona (Figure 1a), with 2767 trees alive in three consecutive NFIs in 322 plots (Table 1). A DBH distribution of these species for each NFI can be found in Figure 1b.

2.2. The Bertalanffy–Chapman–Richards Equation and Data Fitting

The Bertalanffy–Chapman–Richards ordinary differential equation reads as:

$$\frac{d(DBH(t))}{dt} = \left(\eta DBH(t)^{m} - rDBH(t)\right) \tag{1}$$

where DBH(t) stands for the DBH at time t. The biological interpretation of the coefficients of Equation (1) is as follows:

- η: anabolic processes, which are closely linked to bottom-up factors in the environment as resource availability and the ability of an individual to obtain resources [35]. Anabolic processes relate to an individual's phenotypic growth performance, and they are related to photosynthesis [36].
- m: the allometric constant, which is directly related to species-specific growth [37].
- r: the catabolism coefficient, which is related to the energy used for the operation and maintenance of existing tissue [38]. Catabolic factors are proportional to mass [39]. In Coble et al. [36], the product r*DBH was related to catabolic growth processes, such as respiration.

Yuncai et al. [40] concluded that the growth curves of fast-growing forests do not possess an inflection point (apparently because of sustainable growth) expressed by the convex shape. This condition constrains the values of the equation parameters to $m > 0$, and $\eta (1/(1-m) \leq y_0$, being y_0 is the value of the DBH at the initial time; further information on the model coefficient estimates can be found in Appendix A.

Table 1. Ni stands for both the number of individuals (white) alive in the three NFI and the number of plots (grey) used. We considered two aggregation levels (individual (In) and plot-quantile classes (PQ)) and two Equations (1) and (2) (Co for competition) for each of the four species (*Pinus sylvestris*, *Pinus halepensis*, *Pinus nigra*, and *Quercus ilex*) under study.

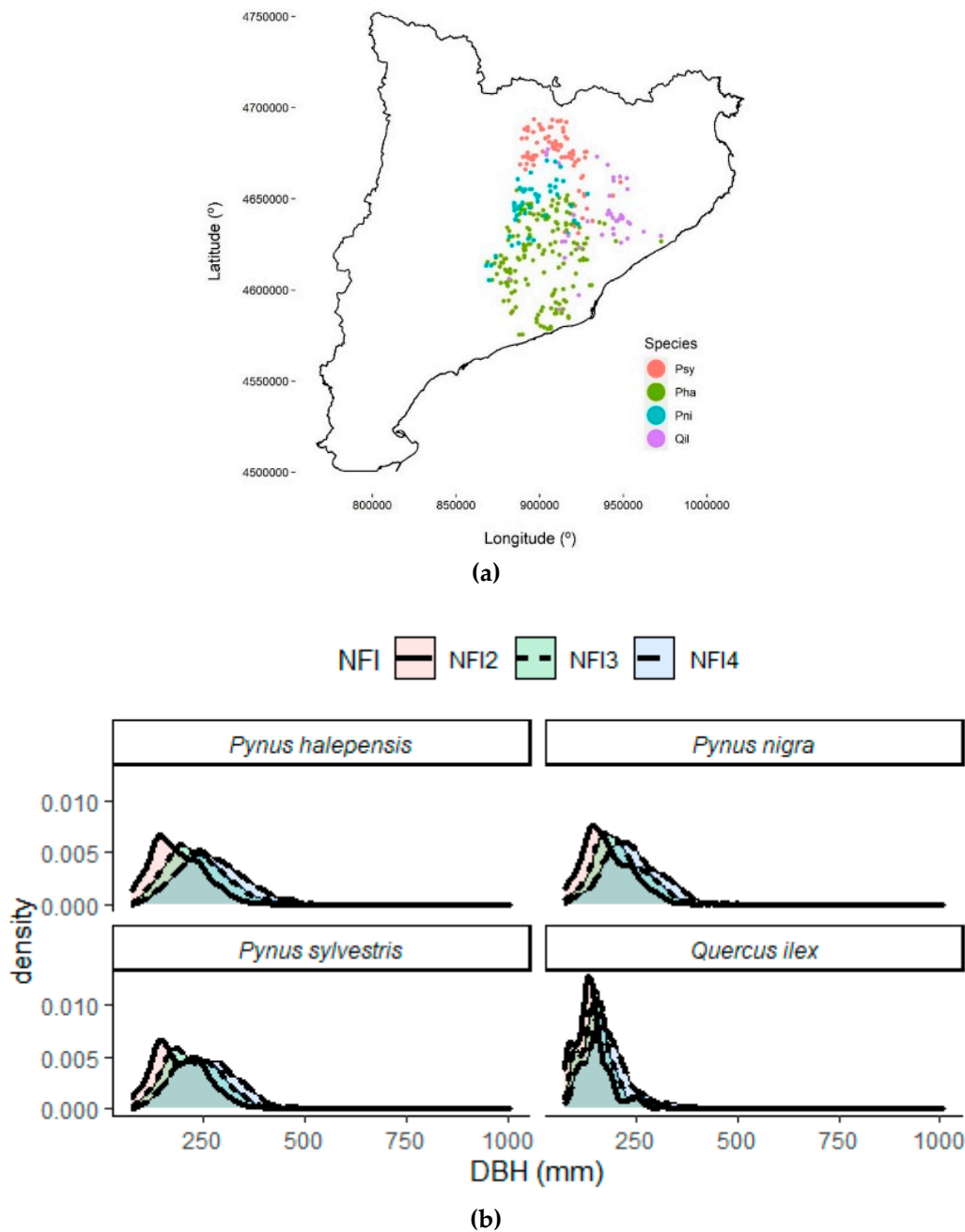| Species	Ni		In		InCo		PQ		PQCo	
Pinus sylvestris	899	77	800 (89%)	75 (97%)	695 (77%)	75 (97%)	802 (89%)	71 (92%)	718 (80%)	72 (94%)
Pinus halepensis	1026	156	976 (95%)	154 (99%)	936 (91%)	154 (99%)	946 (92%)	145 (93%)	949 (92%)	148 (95%)
Pinus nigra	388	4	329 (85%)	44 (94%)	305 (79%)	44 (94%)	322 (83%)	42 (89%)	287 (74%)	41 (87%)
Quercus ilex	454	42	351 (77%)	36 (86%)	275 (61%)	36 (86%)	387 (85%)	34 (81%)	301 (66%)	32 (76%)

(a)

(b)

Figure 1. (**a**) Distribution of the National Forest Inventory plots used in this study, as monospecific plots of *Pinus sylvestris* (Psy), *Pinus halepensis* (Pha), *Pinus nigra* (Pni), and *Quercus ilex* (Qil) distributed in the Barcelona region of Catalonia; (**b**) diameter distribution (DBH, mm) for each species at the second, third, and fourth National Forest Inventory (NFI2, NFI3, and NFI4).

The NFI dataset contained information at both the individual level and the plot level so that fitting could be done at different aggregation levels. It is usual to group individuals in cohorts or diametrical classes to speed up calculations by lowering the computational load [41–43]. We considered even and un-even plots; thus, in order to avoid heterogeneity and to mimic the cohort structure, we heuristically set DBH quantile classes with, at most, 5 individuals per class within each plot. For instance, a plot with 8 individuals consisted of 2 quantile classes that we named plot-quantile.

Competition is a key driver of species dynamics [44,45], and it is not explicitly included in Equation (1). Inspired by Strigul et al. [41] we introduced competition as follows:

$$\frac{d(DBH(t))}{dt} = \left(\eta DBH(t)^m - rDBH(t)\right)\gamma \tag{2}$$

where, γ accounts for intra-species competition and is an adaptation of the species dominance index (used, e.g., in [46]) or the competition for the light parameter used in [41]. As mentioned above, we only selected plots that could be considered monospecific, and, therefore, inter-specific competition was not considered. Intra-specific competition could be determined at the individual and plot-quantile levels. For each individual, the competition coefficient γ in Equation (2) was calculated as the ratio of the basal area of the individual and the total basal area of the individuals inhabiting that plot at the initial time. Thus, γ was dimensionless and ranged from 0 to 1, as the competition parameter in Equation (7) in [41]. At the plot level we defined DBH quantile classes within each plot, and γ was the ratio of the sum of the basal area of individuals belonging to the quantile and the total basal area of the individuals inhabiting that plot (at the initial time).

All the data wrangling, fitting, and analysis were performed with the open-source statistical language R 3.5.3 [47]. We fitted the ODE (regardless of fitting to individuals or quantile plots) by using the ODE function from the deSolve package and the modCost and modFit functions from the FME package [48]. Note that we have not fitted the explicit solution of the differential equation (as, for instance, in Zhang et al. [28]), so this approach was suitable for ODEs with no explicit solution.

2.3. Bertalanffy–Chapman–Richards-Based Model to Predict Tree Growth

Based on the BCR equation, we considered two methods to predict DBH growth across time. Each method was tested at both individual and plot-quantile class levels, with (Equation (1)) and without (Equation (2)) intra-species competition. We set the notation In for individuals, PQ for plot-quantile classes, and Co for competition so that, for instance, InCo stands for an individual level with intra-species competition, and PQCo stands for plot-quantile level with intra-species competition (Equation (2)). Thus, we considered, In, InCo, PQ, and PQCo approaches.

Method 1: for trees that were recorded in NFI 2, 3, and 4. For the four target species, we used the data from the NFIs to fit the BCR equation (rather than its explicit solution) to obtain its parameter values (Appendix A). These coefficients were site-specific, and, therefore, climate conditions were embedded in these parameters. Then, we numerically solved Equations (1) and (2) to predict the DBH value of these recorded individuals at the NFI4 time (expected DBH4). Thus, this method corresponded to objectives (i) and (ii). Furthermore, this procedure was immediately applied to each plot-quantile class by fitting the equation to the quantile class data and using the mean DBH2 of the class as the initial value for the resulting BCR equation so that we fulfilled aim (iii).

To analyze the goodness of our prediction, we compared this expected DBH4 to the corresponding DBH recorded at the NFI4 (observed DBH4). A linear regression for each model prediction and observation was performed in Figure 2 (Measured DBH4 in NFI4 (y-axis) vs. Predicted DBH4 for NFI4 (x-axis)), and the determination coefficient r^2 was calculated (Table 2).
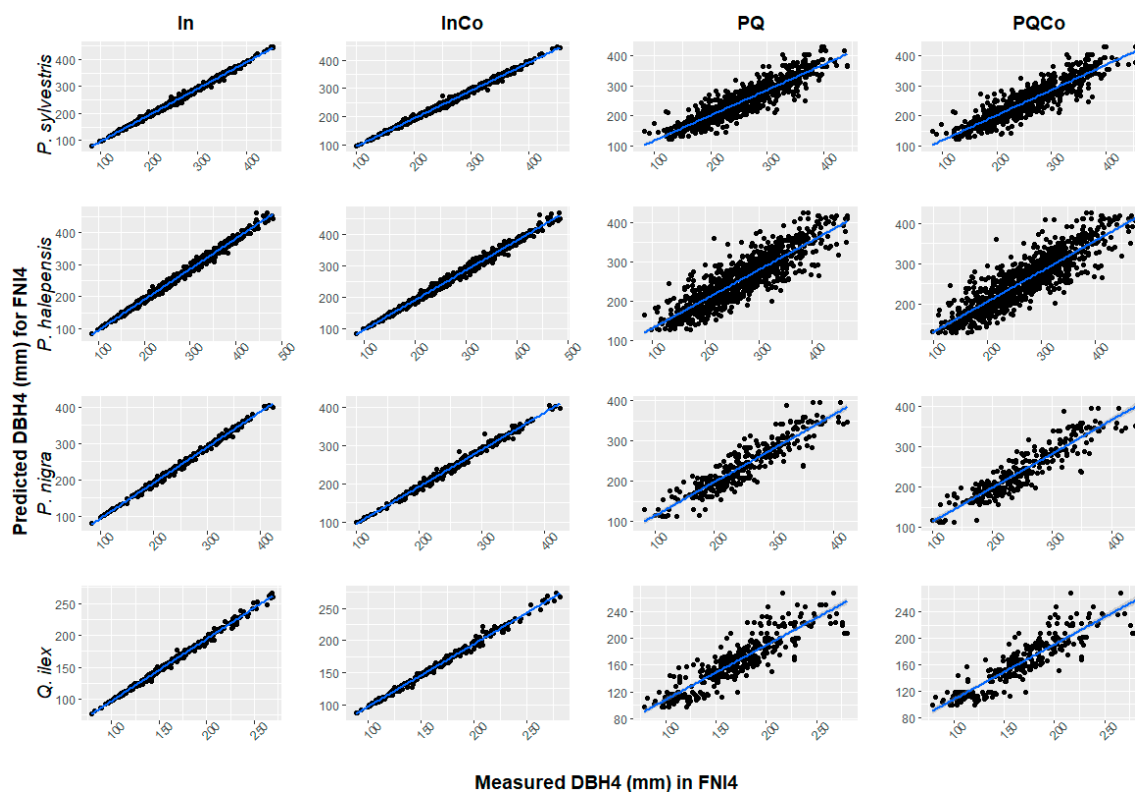
Figure 2. Linear regression line of observed and expected DBH in the fourth National Forest Inventory (DBH4, mm). We considered two aggregation levels (individual and plot-quantile classes), two Equations (1) and (2), and four species (*Pinus sylvestris*, *P. halepensis*, *P. nigra*, and *Quercus ilex*). For the plot quantile aggregation level, the median observed DBH4 was considered for each quantile-plot class instead of the individual observed DBH4.

Table 2. Determination coefficient r^2 was calculated over observed vs. expected DBH for each considered aggregation level (individual (In) and plot-quantile classes (PQ)), Equations (1) and (2) (Co for competition), and species (rows: *Pinus sylvestris*, *P. halepensis*, *P. nigra*, and *Quercus ilex*).

Species	In	InCo	PQ	PQCo
Pinus sylvestris	1.00	0.99	0.98	0.98
Pinus halepensis	1.00	0.99	0.97	0.97
Pinus nigra	0.99	0.99	0.98	0.98
Quercus ilex	1.00	1.00	0.98	0.98

Method 2: for trees for which we only knew their current DBH (which we called "untracked trees"); as a result, they were recorded only once (aim (iv)). We projected the DBH of an untracked individual by using the already calculated parameters of the BCR equation of the most similar individual (in the sense we state next) recorded at three NFI, which we called "the closest neighbour." We defined a distance between two trees based on the following key variables. Following Gomez-Aparicio et al. [49], rainfall (rain, mm) and temperature (T, °C) were the main variables reflecting environment. According to [46,49,50], intra-species competition is a key factor (Co, the γ coefficient defined above, was dimensionless). In addition, basic theorems on differential equations assured that the closest were the initial values (DBH$_{ini}$, mm) and that the closest were the corresponding solution curves of a given ODE. Thus, we defined a distance between two trees A and B as follows:

$$\text{dist}(A, B) = \sqrt{\left(\frac{\text{DBH}_{iniA} - \text{DBH}_{iniB}}{\text{dbh2}_{rank}}\right)^2 + \left(\frac{\text{rainf}_A - \text{rainf}_B}{\text{rainf}_{rank}}\right)^2 + \left(\frac{T_A - T_B}{T_{rank}}\right)^2 + \left(\frac{\text{Co}_A - \text{Co}_B}{\text{Co}_{rank}}\right)^2} \quad (3)$$

The difference between each variable value was normalized by dividing by the range of the corresponding variable (maximum minus minimum). Thus, each term ranged between 0 and 1; it was dimensionless and the maximum theoretical distance was 2. It was straightforward to extend this definition to two plot-quantile classes by considering the mean DBH and mean Co values. The closest neighbour of individual A was the individual B that minimizes the distance. The more similar two objects (trees or quantile classes) were, the smaller the distance value we received. In particular, two individuals or quantile classes A and B were considered to be the same if $dist(A,B) = 0$.

To test the capability of Method 2 to forecast the DBH growth, we proceeded as follows:

1. We randomly split the entire dataset into two blocks: the training set (80% of the available data) and the validation set (the other 20% of the available data).
2. We fed the model by fitting all the individuals (plot-quantile classes) in the training set.
3. For each level (individual or plot-quantile class) belonging to the validation set, we choose its closest neighbour in the training set using Equation (3) (for the DBH component, we considered that in NFI2).
4. We forecasted the DBH at the NFI4 time of this entity of the validation set by using its DBH at NFI2 as the initial value and the model parameters r, m, and η of its closest neighbour (as well as the competition parameter when needed).
5. We then compared the predicted DBH to the actual DBH (which was recorded at NFI4).

We repeated these steps 2000 times for each species, aggregation level, and Equations (1) and (2). Then, we performed a linear regression analysis, comparing observed DBH vs. expected DBH in NFI4, and analyzed the ratios of the observed DBH vs. the expected DBH in NFI4.

We also analyzed the ratios of the expected DBH and the observed DBH4 (ratio = 1 means perfect forecast) of the individuals with only one diameter at three different scales, individuals and plot-quantile classes (level 1), entire plots (level 2), and the whole region (level 3), to detect potential bias and to determine the bounds for the deviation and variability of the estimates when assessing an individual's growth when only one tree size was known. Namely, at level 1, we compared individuals and the mean DBH4 value of each plot-quantile altogether. At level 2, we calculated the ratio of the mean value of the observed DBH4 (through the plot) over the mean value of the expected DBH4 (through the plot) for all the plots through all the 2000 replicas. Finally, at level 3, we calculated the ratio of the mean observed DBH4 and the mean expected DBH4 of all the individuals with measurements chosen in each of the 2000 replicas. Then, after excluding the outliers, we considered 95% of the central ratios (i.e., we cut off the 2.5% of the smaller and larger ratios) at each level.

3. Results

3.1. Modelling and Predicting Tree Growth for Monospecific and Growing Trees and Stands

Our models supported high accuracy in the predictions, as suggested by the linear relationship at the individual aggregation level (i.e., Measured DBH for NFI4 vs. Predicted DBH for NFI4 for each individual, Figure 2) and at the quantile-plot aggregation level, (i.e., the mean Measured DBH for NFI4 of the quantile vs. the Predicted DBH for NFI4 of the quantile, Figure 2). The assumptions of the linear model of the Measured vs. the Predicted DBH for NFI4 were met (Appendix B). The slopes of the corresponding linear models were close to 1, and the intercepts were close to 0, for all the four species and models parameterized (Appendix B), and the determination coefficients r^2 ranged from 0.97 to 1 (Table 2).

3.2. Predicting Tree Growth for Trees with Only One DBH Measurement (Untracked Individuals)

We tested the accuracy of the predictions using the closest neighbour (aim (iii)) by calculating the r^2 coefficient of the linear regression model (Figure 3) of the measured DBH in FNI4 (calculated with the closest neighbour) vs. the Predicted DBH for FNI4(Method 2,

see Table 3). Overall, we found r² ranging from 0.70 to 0.83. The assumptions of the linear model were met (Appendix C). The slopes of the corresponding linear models were close to 1, and the intercepts were close to 0, for all the four species and models parameterized (Appendix C).
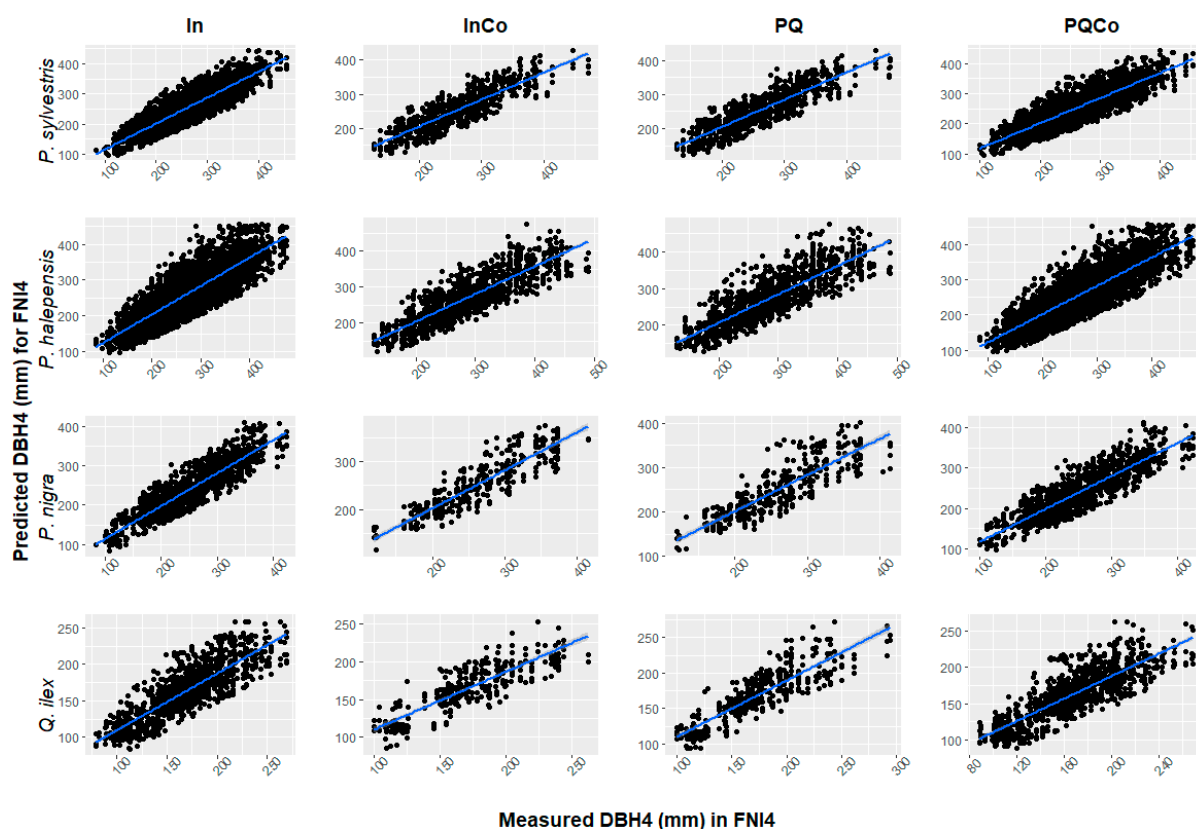

Figure 3. Linear regression line of expected versus observed tree size in the fourth National Forest Inventory (DBH4, mm) with the closest neighbour for aggregation levels (individual and plot-quantile classes), two Equations (1) and (2), and species (*Pinus sylvestris*, *P. halepensis*, *P. nigra*, and *Quercus ilex*).

Table 3. Determination of coefficient r² of the linear model relating observed DBH vs. expected DBH at NFI4 with the closest neighbour for each aggregation level (individual (In) and plot-quantile classes (PQ)), Equations (1) and (2) (Co for competition), and species (*Pinus sylvestris*, *Pinus halepensis*, *Pinus nigra*, and *Quercus ilex*).

Species	In	InCo	PQ	PQCo
Pinus sylvestris	0.82	0.79	0.80	0.80
Pinus halepensis	0.70	0.75	0.72	0.72
Pinus nigra	0.83	0.80	0.73	0.81
Quercus ilex	0.74	0.74	0.72	0.71

The ratio between the observed and the predicted was centered almost at 1 in all the aggregation levels. Although there was systematic bias towards a greater value for the observed than the predicted DBH (the center point was slightly larger than 1 in all the panels in Figure 4), it was always less than a 5% deviation. As expected, the variability in the ratios decreased as the aggregation level increased (from up to 40% (individual level, Figure 4a) to less than 10% (regional level, Figure 4c)).
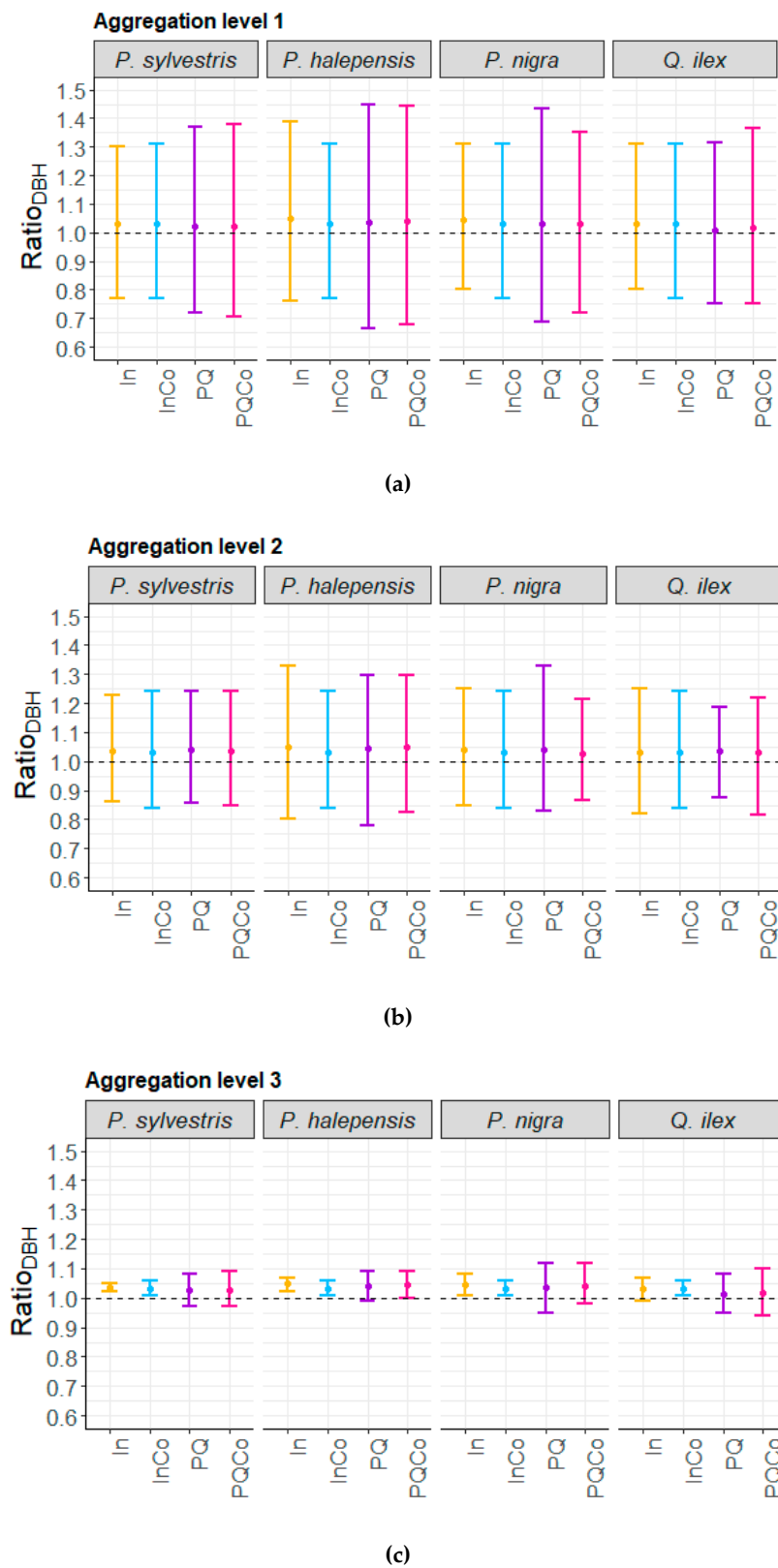
(a)

(b)

(c)

Figure 4. Ratio of predicted over observed DBH for 95% of the data for three resolution levels: individual (In) and plot-quantile (PQ) (i.e., level 1, (**a**)), plot (level 2, (**b**)), and the whole area of the studio (level 3, (**c**)), considering two aggregation levels (individual and plot-quantile classes), two Equations (1) and (2) (Co for competition), and four species (*Pinus sylvestris*, *Pinus halepensis*, *Pinus nigra*, and *Quercus ilex*).

3.3. Basal Area Estimates

We also calculated the BA from the DBH by using the circle area formula. The relationship between the observed and the expected basal area for individuals with three measurements (Method 1) produced, for each species and aggregation level, an r^2 of at least 0.96 (see Appendix D, Table A3). For individuals with only one tree diameter measurement, it varied from 0.66 to 0.81 (see Appendix D, Table A5).

4. Discussion

The BCR model is an analytical approximation that lies between process-based and empirical models, which are the edges of a continuum of models' classification [17,22]. Thus, it retains features of both types of models: it is a predictive (extrapolative) model [24] that requires fewer parameters and a lower computational effort than process-based models, making it a suitable option for decision support and prospective analyses [24,29]. Yet, unlike polynomial growth models, it is biologically interpretable as its coefficients are related to plant growth through anabolic and catabolic processes (see the references in Section 2.2). As more observations are available across spatial and temporal scales and levels of biological organization [17], and as computation capability increases, data-driven empirical models offer a unique opportunity to describe general patterns and regularities in complex data sets.

We have found that the BCR equation is a reliable distance-independent individual-tree growth model with just three DBH records, fulfilling aim (i). Both the BCR model (which is an ODE) and the generalized algebraic difference approach (GADA) [30] belong to the class of dynamic equations [24]. GADA models have been shown to be reliable in predicting tree growth [29,51,52], although building up the whole model and fitting it is not as straightforward as it is with ODEs. We found that the BCR model applied in the Barcelona region (Spain) for the above-mentioned species produced DBH (see Section 3) and BA predictions (see Appendix D) as accurate as in Castedo-Dorado [52], which used the GADA with length 5 temporal series, or in Barrio-Anta [51], which also used the GADA with length 2 up to length 12 temporal series. In addition, and in contrast to GADA models, the BCR model (and, generally, ODEs) does not require specific local information such as a site quality index, which is not easily available at a regional scale [29]. Another important advantage of the BCR model is that, unlike tree-ring-based-models, which project growth-climate trends without considering the specific effect of tree size [53], the initial tree size was included in the tree growth calculation.

Our BCR parameterisation of tree growth with NFI data can also be compared to phenomenological models and yield tables largely used to understand or predict tree growth. For instance, Rohner et al. [54] used the three Swiss NFI to predict individual BA across time. Instead of the BCR equation, they used nonlinear mixed-models and up to 16 explanatory variables to assess BA dynamics, in contrast to the three coefficients of the BCR model to model the DBH (which yields BA); furthermore, Table A3 in Appendix D shows that the BCR model is more explanatory (i.e., r^2) using Method 1. However, one advantage of BCR in contrast to the phenomenological (correlational) models is the temporal prediction beyond the data used to parameterise. On the other hand, yield tables project target stand characteristics with the parameterisation of local stand data from cohorts, in order to obtain suitable forest production estimates (e.g., [55]). However, they have turned out to not be flexible enough to dynamically simulate stand development and the evaluation of the effects of different management alternatives [56,57]. The BCR model has also been easily adapted to perform calculations considering cohorts, which have been found particularly useful for applications in large areas [41]. In fact, if we compare aggregation levels (individual and plot-quantile, with and without competition) in Table 2 (for Method 1, i.e., temporal predictions) and in Table 3 (for Method 2, i.e., spatiotemporal predictions), we obtained similar accuracy predictions for either individual or cohort-like data, fulfilling objective (ii). Integral projection models (IPM) have also been parameterised with data from forest inventories to obtain a forest DBH distribution model, where the

individual growth law used was phenomenological. For instance, Kunstler et al. [58] used data from 27 species across Europe. Although they only used two data temporal series, they analyzed a wide range of DBH. Therefore, they could predict DBH growth for any initial DBH. An IPM was developed with Spanish NFI (2 and 3) in García-Callejas et al. [59]. IPMs are probabilistic models (unlike our models, which are deterministic), and survival and reproduction are also considered.

With the spatiotemporal predictions (Method 2) we could predict tree growth for individuals or plot-quantiles of plots that have not been previously recorded. Prediction accuracy for tree size was lower than temporal predictions (Method 1): for instance, we found $r^2 > 0.97$ (see Table 2) with Method 1, whereas Method 2 yielded $0.71 < r^2 < 0.82$ (see Table 3). Other studies, such as Rohner et al. [54], have predicted basal area values for trees that have not been previously recorded with different estimate. Our Method 2 yielded $0.66 < r^2 < 0.81$, depending on the species, the aggregation level, and whether we used Equation (1) or (2) (see Table A5 in Appendix D), whereas Rohner et al. found $r^2 < 0.2$ (in [54]). Therefore, and fulfilling the third objective (iii), the spatiotemporal predictions (Method 2) can be used to predict tree growth in plots with at least one NFI.

Finally, regarding the fourth objective (iv) of considering intra-species competition, equation (2) did not significantly improve the fitting. Many studies have found that both intraspecific competition and climate are key determinants of tree growth and stand dynamics (see, e.g., [11,49]). Yet, competition can be relatively low in stands at initial developing stages, particularly in even-aged stands (e.g., [60]). Accordingly, competitive effects may arise at later stages.

5. Caveats and Further Work

This ODE model parameterised with three consecutive NFIs can be used in different directions in the future, ranging from prediction to understanding under key determinants of tree growth. In the ODE use for tree growth predictions, the availability of forest inventories are key to parameterise empirical data-driven models of tree and stand growth dynamics. The estimation of local and regional carbon pools can be used by private owners and policy makers to evaluate short-term trends under different scenarios (i.e., afforestation, abandonment, or a particular management). Systematic data, such as the national forest inventories, provide an excellent opportunity for public administrations and stakeholders to better monitor and predict biomass and above-ground carbon stocks in existing forests. Tree growth dynamics can be used along with volumetric formulae or allometric relations to predict timber yield (as in [52]) or carbon storage [28]. Additionally, other ODE models can be fitted to obtain tree height dynamics and to complete forest dynamics information. On the other hand, the use of ODE models can be used to further understand species-specific responses and processes underlying tree growth. There is a clear biological and physiological interpretation for the coefficients of the BCR equation (see Section 2.2). A natural question is whether these coefficients characterize species and functional groups or whether they depend on explanatory variables (e.g., climate or geographical variables), because we did not find strong species-specific differences.

Our method should be applied to monospecific forests in which tree growth—rather than recruitment and mortality—is the main underlying driver of stand carbon balance (e.g., young plantations without a strong self-thinning component). To further apply these methods in other forest types and longer time scales (i.e., from decades to centuries), key demographic processes such as recruitment and mortality should be included as a key component of forest carbon dynamics [61,62] as well as other metrics of biotic [58] and abiotic [63] interactions.

Appendix A

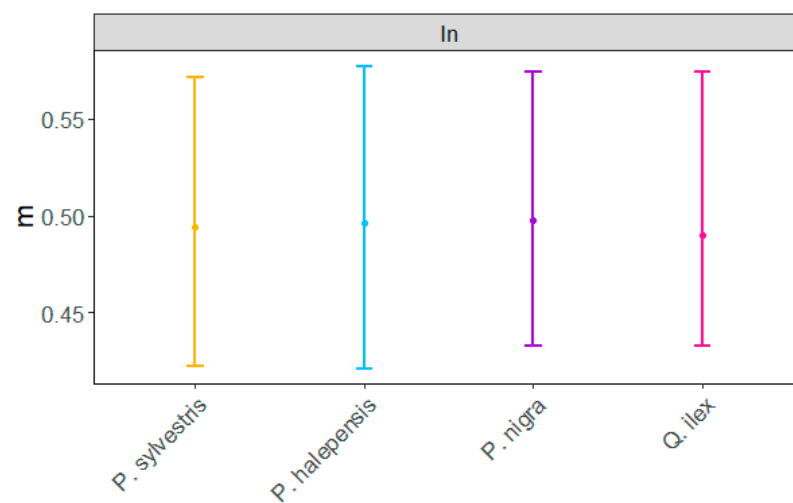For each coefficient in Equation (1) and each species, bars in Figure A1 stand for the 95% level of the central values of each coefficient in Equation (1) calculated on each individual of each species (that is, we cut off the 2.5% levels of the smaller and larger parameter values). Let us note that introducing competition, as in Equation (2), resulted in a great amount of variability, as well as grouping individuals in quantile classes; so, we did not include these cases.
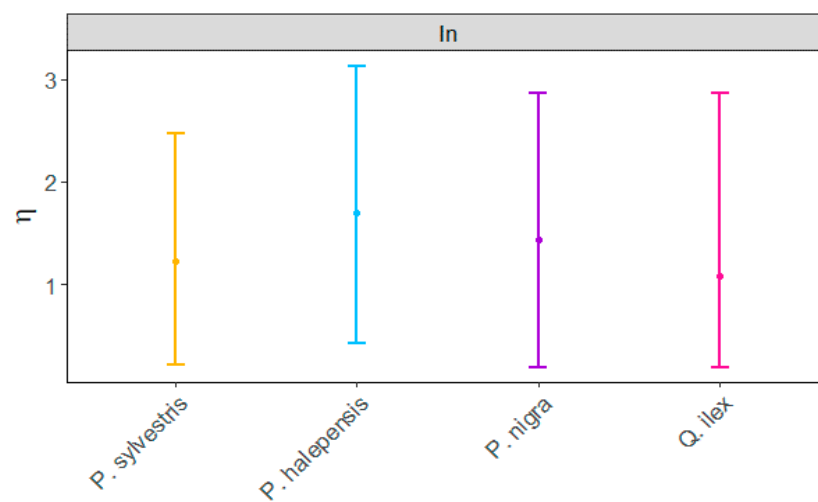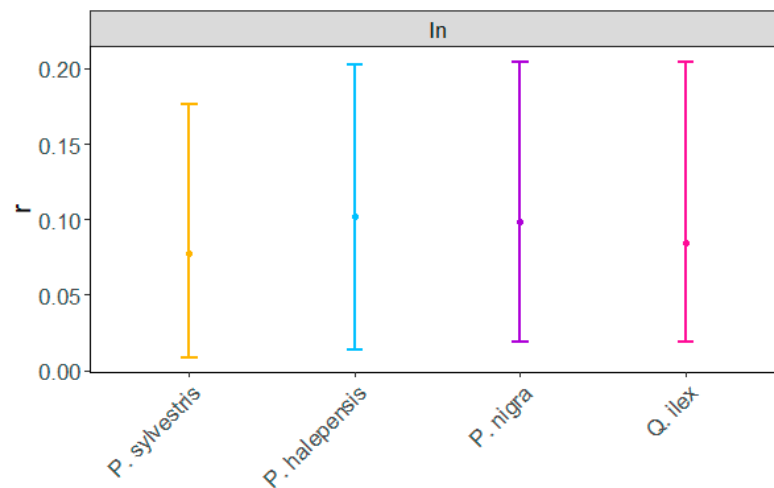

(a)

Figure A1. *Cont.*

(b)

(c)

Figure A1. Bars with the 95% level of the central values for each coefficient in Equation (1) (panels (**a**–**c**) correspond, respectively, to coefficient η, m and r) and each species calculated at the individual (In) level.

Appendix B

Diagnostic plots for the linear model assumptions for observed DNH4 and expected DBH4: Figure A2 displays qqplots and Figure A3 shows the residuals vs. the fitted values for each species, aggregation level (individual (In) and plot-quantile classes (PQ)), and Equations (1) and (2) (Co for competition). Essentially, linear model assumptions were met. Besides, Table A1 gathers the confidence interval at the 95% level for the intercept and for the slope of the linear model between the observed DBH4 and the expected DBH4 for tracked trees.
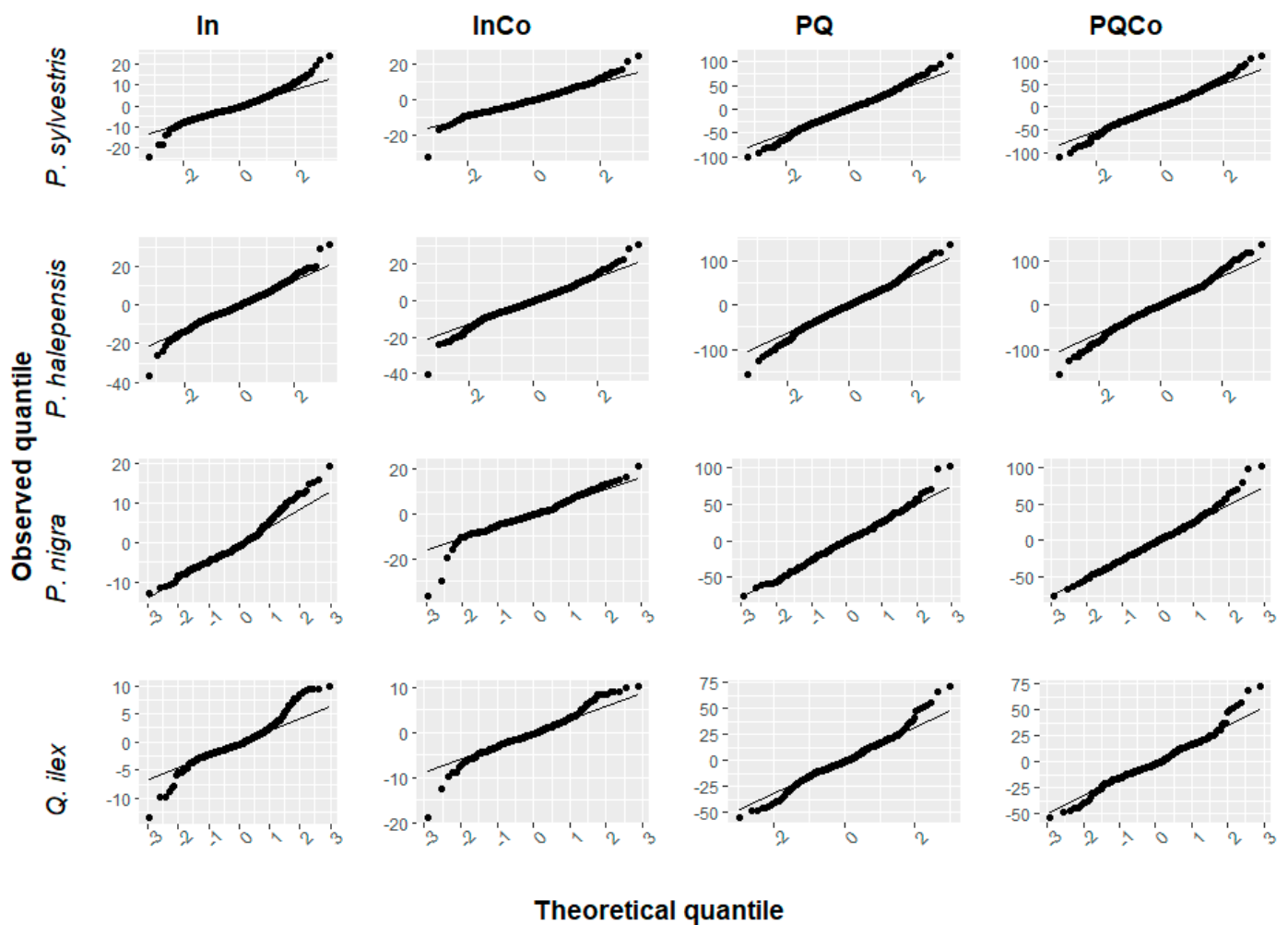
Figure A2. Diagnostic plots (qqplots) of the linear model for observed DBH4 vs. predicted DBH4 for each aggregation level (individual (In) and plot-quantile classes (PQ)), two Equations (1) and (2) (Co for competition), and four species (*Pinus sylvestris*, *P. halepensis*, *P. nigra*, and *Quercus ilex*).
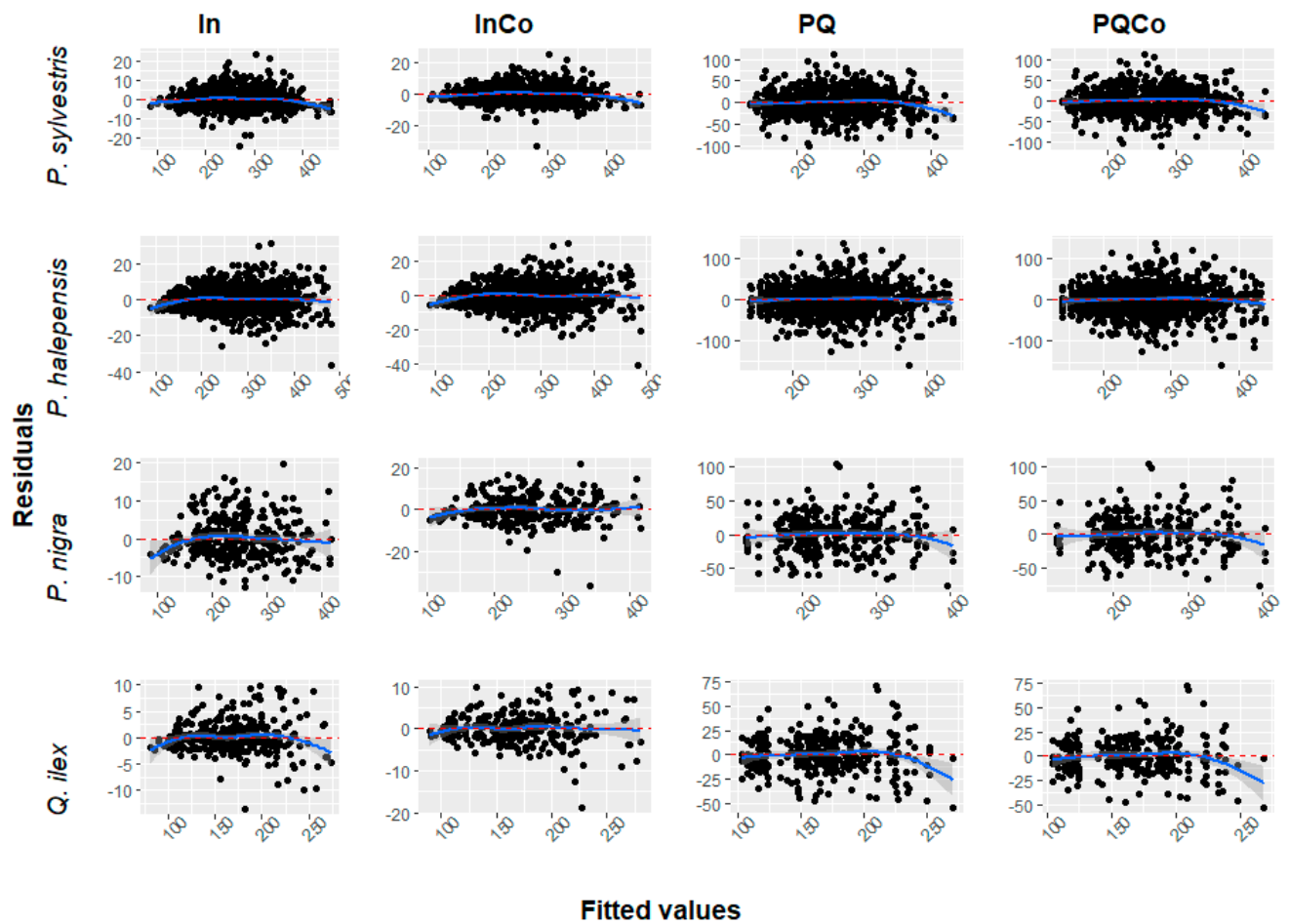
Figure A3. Diagnostic plot (residual vs. fitted values) of the linear model for observed DBH4 vs. predicted DBH4 for the two aggregation levels (individual and plot-quantile classes), Equations (1) and (2), and the four species (*Pinus sylvestris, P. halepensis, P. nigra,* and *Quercus ilex*).

Table A1. Confidence interval at the 95% level for the intercept and for the slope of the linear model between the observed and the expected DBH4 for tracked trees, the two aggregation levels (individual (In) and plot-quantile classes (PQ)), Equations (1) and (2) (Co for competition), and the four species (*Pinus sylvestris, P. halepensis, P. nigra,* and *Quercus ilex*).

	Regression Line Coefficient	In	InCo	PQ	PQCo
Pinus sylvestris	intercept	(1.87, 4.41)	(2.46, 5.58)	(2.63, 18.87)	(1.57, 19.33)
	slope	(1.01, 1.02)	(1.01, 1.02)	(0.95, 1.02)	(0.95, 1.02)
Pinus halepensis	intercept	(1.52, 4.74)	(1.45, 4.52)	(0.23, 19.90)	(1.69, 20.99)
	slope	(1.03, 1.04)	(1.03, 1.04)	(0.97, 1.05)	(0.97, 1.04)
Pinus nigra	intercept	(1.73, 5.99)	(2.79, 8.40)	(−2.58, 21.35)	(−1.89, 23.28)
	slope	(1.01, 1.03)	(1.00, 1.03)	(0.95, 1.05)	(0.94, 1.05)
Quercus ilex	intercept	(−0.16, 2.73)	(−0.85, 3.07)	(−0.15, 16.96)	(0.51, 19.25)
	slope	(1.01, 1.03)	(1.01, 1.03)	(0.92, 1.03)	(0.91, 1.02)

Appendix C

Diagnostic plots for the linear model assumptions for the observed and the predicted DBH4 for untracked individuals using the closest neighbour (see Section 2.3). Figure A4 displays qqplots and Figure A5 shows the residuals vs. the fitted values for each species, aggregation level, and Equations (1) and (2). Essentially, linear model assumptions were met.
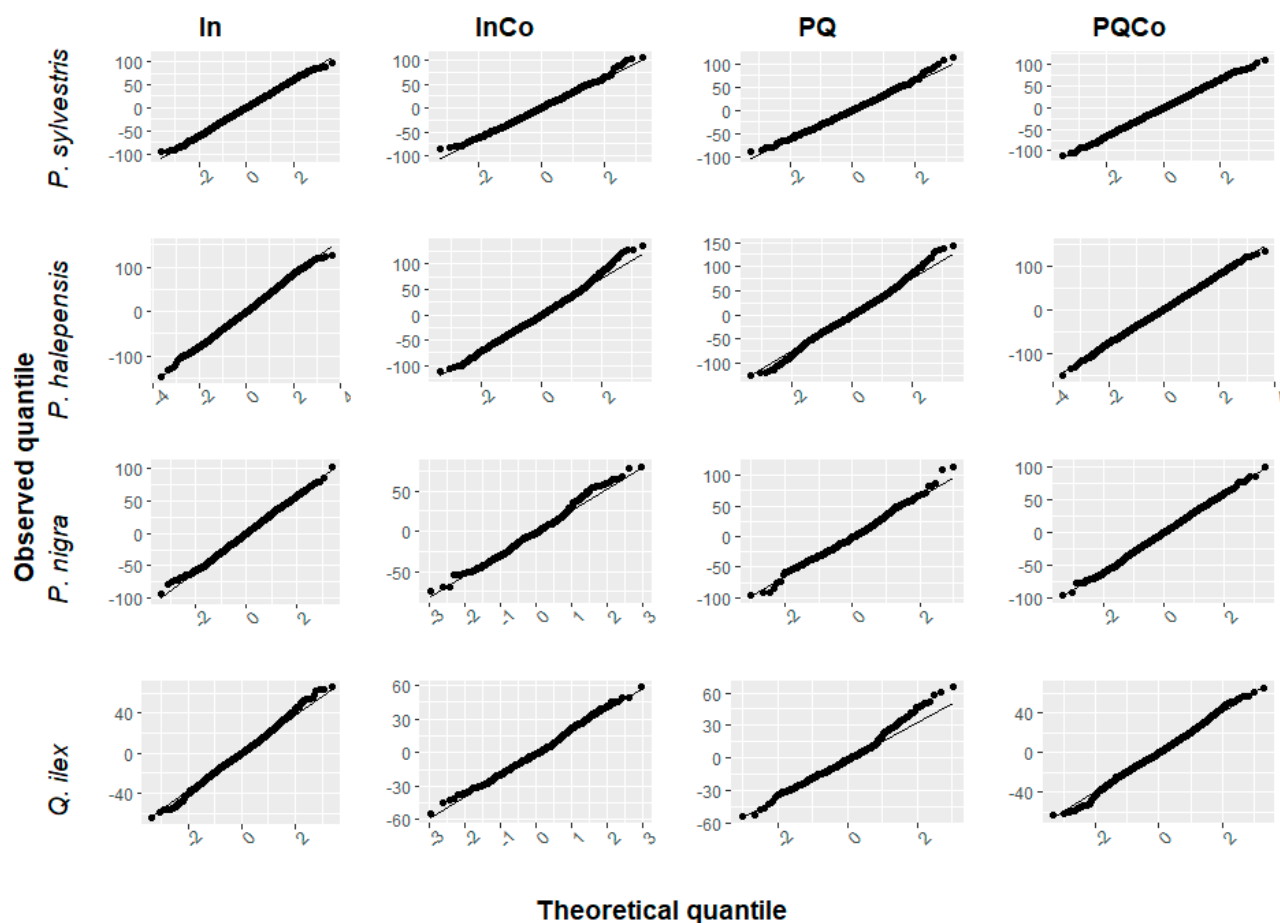

Figure A4. Diagnostic plot (qqplots) of the linear model for observed DBH4 vs. predicted DBH4 with the closest neighbor, plot for each method and species.

Table A2. Confidence interval at the 95% level for the intercept and for the slope of the linear model between the observed DBH4 and the predicted DBH4 for untracked trees considering two aggregation levels (individual (In) and plot-quantile classes (PQ)), and Equations (1) and (2) (Co for competition).

|	Regression Line Coefficient	In	InCo	PQ	PQCo
Pinus sylvestris	intercept	(17.35, 25.49)	(7.34, 27.08)	(7.99, 26.66)	(21.32, 30.71)
	slope	(0.92, 0.95)	(0.92, 1.00)	(0.92, 1.00)	(0.91, 0.94)
Pinus halepensis	intercept	(36.82, 46,37)	(15.00, 32.72)	(25.04, 43.34)	(34.48, 0.94)
	slope	(0.86, 0.90)	(0.93, 1)	(0.88, 0.95)	(0.97, 0.91)
Pinus nigra	intercept	(9.2, 21.51)	(2.14, 30.28)	(24.83, 53.92)	(12.22, 25.73)
	slope	(0.95, 1.00)	(0.92, 1.03)	(0.82, 0.93)	(0.93, 0.99)
Quercus ilex	intercept	(12.59, 22.83)	(1.96, 23.43)	(4.00, 22.41)	(12.32, 25.72)
	slope	(0.89, 0.95)	(0.89, 1.02)	(0.89, 1.00)	(0.84, 0.92)
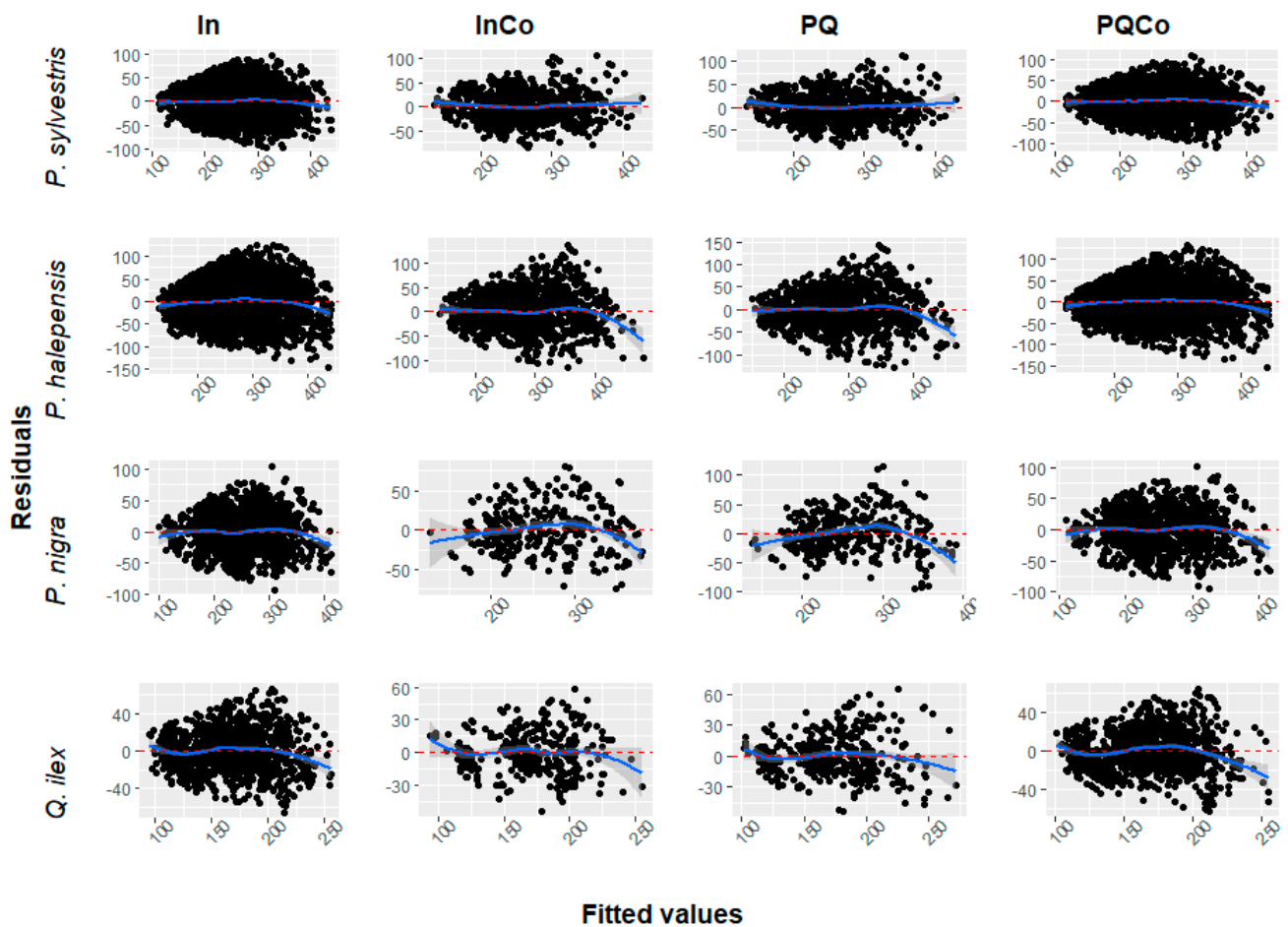
Figure A5. Diagnostic plot (residual vs. fitted values) of the linear model for observed vs. predicted DBH4 with the closest neighbor, plot for each method and species.

Appendix D

Appendix D.1. Basal Area Estimations for Tracked Individuals

We calculated the observed basal area with the measured diameter in the NFI4 and the expected basal area at the individual and quantile-plot levels (level 1) for each plot code. Then, we calculated the linear model (the expected BA vs. the observed BA) for each species, aggregation level, and Equations (1) and (2).

Table A3. Determination coefficient r^2 calculated over expected BA vs. observed BA by species, aggregation level (individual (In) and plot-quantile classes (PQ)), and Equations (1) and (2) (Co for competition).

| Species	In	InCo	PQ	PQCo
Pinus sylvestris	1.00	0.99	1.00	1.00
Pinus halepensis	1.00	0.99	1.00	0.99
Pinus nigra	0.99	0.96	0.99	0.99
Quercus ilex	0.99	0.98	1.00	0.97

Table A4. Intercept of linear model over predicted BA vs. observed BA (mm^2) by species, aggregation level (individual (In) and plot-quantile classes (PQ)), and Equations (1) and (2) (Co for competition).

	Regression Line Coefficient	In	InCo	PQ	PQCo
Pinus sylvestris	intercept	(1.87, 4.41)	(2.63, 18.87)	(1.52, 4.74)	(1.45, 4.82)
	slope	(1.01, 1.02)	(1.01, 1.02)	(0.95, 1.02)	(0.95, 1.02)
Pinus halepensis	intercept	(0.23, 19.90)	(1.69, 20.99)	(1.73, 5.99)	(−2.79, 8.40)
	slope	(1.03, 1.04)	(1.03, 1.04)	(0.97, 1.05)	(0.97, 1.04)
Pinus nigra	intercept	(−2.58, 21.35)	(−1.89, 23.28)	(−0.16, 2.73)	(−1.89, 23.28)
	slope	(1.01, 1.03)	(1.01, 1.03)	(0.95, 1.05)	(0.94, 1.05)
Quercus ilex	intercept	(−0.16, 2.73)	(−0.85, 3.07)	(−0.49, 16.73)	(0.05, 18.99)
	slope	(1.01, 1.03)	(1.01, 1.03)	(0.93, 1.03)	(0.91, 1.02)

Appendix D.2. Validating Basal Area Estimation: Expected Basal Area for Untracked Individuals

Table A5. Determination coefficient r^2 calculated over expected BA vs. observed BA by species, aggregation level (individual (In) and plot-quantile classes (PQ)), and Equations (1) and (2) (Co for competition); calculations done at individual level with untracked individuals.

BA Linear Model r^2 Species	In	InCo	PQ	PQCo
Pinus sylvestris	0.81	0.79	0.79	0.79
Pinus halepensis	0.68	0.70	0.72	0.72
P inus nigra	0.81	0.79	0.79	0.79
Quercus ilex	0.71	0.66	0.70	0.70
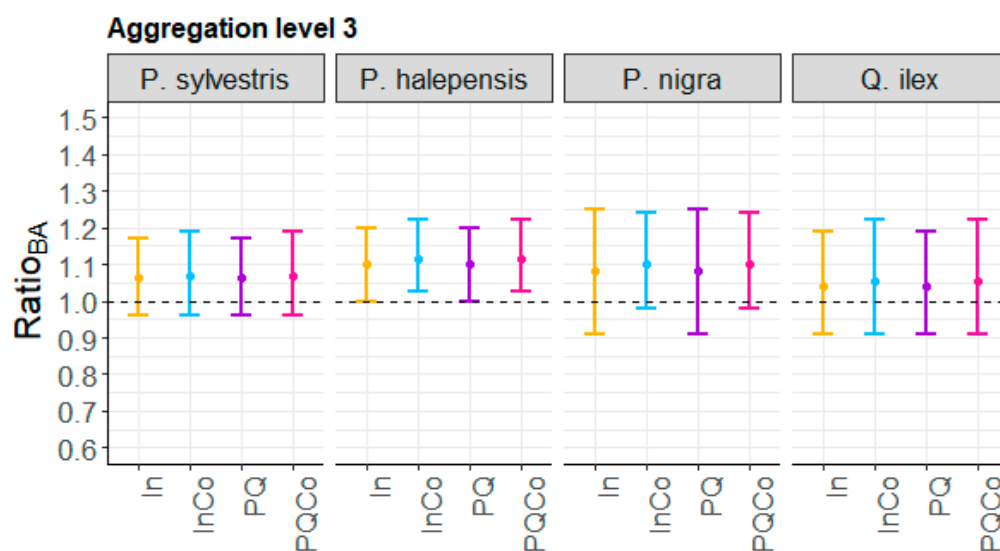
Figure A6. Each bar consists of central 95% ratio (we cut off the 2.5% levels of the smallest and largest ratios) of the total predicted basal area and the total observed basal area over the validation set for the region of Barcelona calculated over the 2000 replicas (see Section 2.3) for each species and model.

References

1. Millennium Ecosystem Assessment. *Ecosystem and Human Well-Being: Biodiversity Synthesis*; World Resources Institute: Washington, DC, USA, 2005.
2. IPBES. *Global Assessment Report on Biodiversity and Ecosystem Services of the Intergovernmental Science-Policy Platform on Biodiversity and Ecosystem Services*; Brondizio, E.S., Settele, J., Diaz, S., Ngo, H.T., Eds.; IPBES Secretariat: Bonn, Germany, 2019.
3. Harris, N.L.; Gibbs, D.A.; Baccini, A.; Birdsey, R.A.; de Bruin, S.; Farina, M.; Fatoyinbo, L.; Hansen, M.C.; Herold, M.; Houghton, R.A.; et al. Global maps of twenty-first century forest carbon fluxes. *Nat. Clim. Chang.* **2021**, *11*, 234–240. [CrossRef]

4. Song, X.-P.; Hansen, M.C.; Stehman, S.V.; Potapov, P.V.; Tyukavina, A.; Vermote, E.F.; Townshend, J.R. Global land change from 1982 to 2016. *Nature* **2018**, *560*, 639–643. [CrossRef]

5. Pan, Y.; Birdsey, R.A.; Fang, J.; Houghton, R.; Kauppi, P.E.; Kurz, W.A.; Phillips, O.; Shvidenko, A.; Lewis, S.L.; Canadell, J.; et al. A Large and Persistent Carbon Sink in the World's Forests. *Science* **2011**, *333*, 988–993. [CrossRef]

6. Cohen-Shacham, E.; Janzen, C.; Maginnis, S.; Gretchen, E. *Nature-Based Solutions to Address Global Societal Challenges*; IUCN: Gland, Switzerland, 2016.

7. Van Der Plas, F.; Ratcliffe, S.; Ruiz-Benito, P.; Scherer-Lorenzen, M.; Verheyen, K.; Wirth, C.; Zavala, M.; Ampoorter, E.; Baeten, L.; Barbaro, L.; et al. Continental mapping of forest ecosystem functions reveals widespread synergies. *Ecol. Lett.* **2017**, *21*, 31–42. [CrossRef]

8. Mäkelä, A.; del Río, M.; Hynynen, J.; Hawkins, M.J.; Reyer, C.; Soares, P.; van Oijen, M.; Tomé, M. Using stand-scale forest models for estimating indicators of sustainable forest management. *For. Ecol. Manag.* **2012**, *285*, 164–178. [CrossRef]

9. Shifley, S.R.; He, H.S.; Lischke, H.; Wang, W.J.; Jin, W.; Gustafson, E.J.; Thompson, J.R.; Thompson, F.R.; Dijak, W.D.; Yang, J. The past and future of modeling forest dynamics: From growth and yield curves to forest landscape models. *Landsc. Ecol.* **2017**, *32*, 1307–1325. [CrossRef]

10. Coomes, D.A.; Allen, R.B. Effects of size, competition and altitude on tree growth. *J. Ecol.* **2007**, *95*, 1084–1097. [CrossRef]

11. Marqués, L.; Camarero, J.J.; Zavala, M.A.; Stoffel, M.; Ballesteros-Cánovas, J.A.; Sancho-García, C.; Madrigal-González, J. Evaluating tree-to-tree competition during stand development in a relict Scots pine forest: How much does climate matter? *Trees* **2021**, 1–13. [CrossRef]

12. Sabaté, S.; Gracia, C.A.; Sánchez, A. Likely effects of climate change on growth of Quercus ilex, Pinus halepensis, Pinus pinaster, Pinus sylvestris and Fagus sylvatica forests in the Mediterranean region. *For. Ecol. Manag.* **2002**, *162*, 23–37. [CrossRef]

13. Zavala, M.A.; Espelta, J.M.; Caspersen, J.; Retana, J. Interspecific differences in sapling performance with respect to light and aridity gradients in Mediterranean pine–oak forests: Implications for species coexistence. *Can. J. For. Res.* **2011**, *41*, 1432–1444. [CrossRef]

14. Caspersen, J.P.; Kobe, R.K. Interspecific variation in sapling mortality in relation to growth and soil moisture. *Oikos* **2001**, *92*, 160–168. [CrossRef]

15. Kohyama, T. Density-size Dynamics of Trees Simulated by a One-sided Competition Multi-species Model of Rain Forest Stands. *Ann. Bot.* **1992**, *70*, 451–460. [CrossRef]

16. Sánchez-Gómez, D.; Zavala, M.A.; Van Schalkwijk, D.B.; Urbieta, I.R.; Valladares, F. Rank reversals in tree growth along tree size, competition and climatic gradients for four forest canopy dominant species in Central Spain. *Ann. For. Sci.* **2008**, *65*, 605. [CrossRef]

17. Ruiz-Benito, P.; Vacchiano, G.; Lines, E.R.; Reyer, C.P.; Ratcliffe, S.; Morin, X.; Hartig, F.; Mäkelä, A.; Yousefpour, R.; Chaves, J.E.; et al. Available and missing data to model impact of climate change on European forests. *Ecol. Model.* **2020**, *416*, 108870. [CrossRef]

18. Lindner, M.; Fitzgerald, J.; Zimmermann, N.E.; Reyer, C.; Delzon, S.; van der Maaten, E.; Schelhaas, M.-J.; Lasch, P.; Eggers, J.; van der Maaten-Theunissen, M.; et al. Climate change and European forests: What do we know, what are the uncertainties, and what are the implications for forest management? *J. Environ. Manag.* **2014**, *146*, 69–83. [CrossRef]

19. Blanco, J.A.; Ameztegui, A.; Rodríguez, F. Modelling Forest Ecosystems: A crossroad between scales, techniques and applications. *Ecol. Model.* **2020**, *425*, 109030. [CrossRef]

20. Ruizbenito, P.; Madrigalgonzalez, J.; Ratcliffe, S.J.; Coomes, D.A.; Kandler, G.; Lehtonen, A.; Wirth, C.; Zavala, M.A. Stand Structure and Recent Climate Change Constrain Stand Basal Area Change in European Forests: A Comparison Across Boreal, Temperate, and Mediterranean Biomes. *Ecosystems* **2014**, *17*, 1439–1454. [CrossRef]

21. Nabuurs, G.-J.; Schelhaas, M.-J.; Mohren, G.M.J.; Field, C.B. Temporal evolution of the European forest sector carbon sink from 1950 to 1999. *Glob. Chang. Biol.* **2003**, *9*, 152–160. [CrossRef]

22. Korzukhin, M.D.; Ter-Mikaelian, M.T. An individual tree-based model of competition for light. *Ecol. Model.* **1995**, *79*, 221–229. [CrossRef]

23. Dale, V.; Doyle, T.; Shugart, H. A comparison of tree growth models. *Ecol. Model.* **1985**, *29*, 145–169. [CrossRef]

24. García, O. Stand growth models: Theory and practice. In Advancement in Forest Inventory and Forest Management Sciences, Proceedings of the IUFRO Seoul Conference, Seoul, Korea, 20–25 September 1993; Springer: Dordrecht, The Netherlands, 1993; pp. 22–45.

25. Von Bertalanffy, L. Quantitative Laws in Metabolism and Growth. *Q. Rev. Biol.* **1957**, *32*, 217–231. [CrossRef]

26. Richards, F.J. A Flexible Growth Function for Empirical Use. *J. Exp. Bot.* **1959**, *10*, 290–301. [CrossRef]

27. Liu, Z.-G.; Li, F.-R. The generalized Chapman-Richards function and applications to tree and stand growth. *J. For. Res.* **2003**, *14*, 19–26. [CrossRef]

28. Zhang, C.; Ju, W.; Chen, J.; Fang, M.; Wu, M.; Chang, X.; Wang, T.; Wang, X. Sustained Biomass Carbon Sequestration by China's Forests from 2010 to 2050. *Forests* **2018**, *9*, 689. [CrossRef]

29. Álvarez-González, J.G.; Cañellas, I.; Alberdi, I.; Gadow, K.; Ruiz-González, A. National Forest Inventory and forest observational studies in Spain: Applications to forest modeling. *For. Ecol. Manag.* **2014**, *316*, 54–64. [CrossRef]

30. Cieszewski, C.J.; Bailey, R.L. Generalized algebraic difference approach: Theory based derivation of dynamic site equations with polymorphism and variable asymptotes. *For. Sci.* **2000**, *46*, 116–126.

31. Villaescusa, R.; Díaz, R. *Segundo Inventario Forestal Nacional (1986–1996)*; Ministerio de Medio Ambiente, ICONA: Madrid, Spain, 1998.

32. Alberdi, I.; Vallejo, R.; Álvarez-González, J.G.; Condés, S.; González-Ferreiro, E.; Guerrero, S.; Hernández, L.; Martínez-Jauregui, M.; Montes, F.; Oliveira, N.; et al. The multi-objective Spanish National Forest Inventory. *For. Syst.* **2017**, *26*, e04S. [CrossRef]

33. Gonzalo Jiménez, J. *Diagnosis Fitoclimática de la España Peninsular: Hacia un Modelo de Clasificación Funcional de la Vegetación y de los Ecosistemas Peninsulares Españoles*; Organismo Autónomo de Parques Nacionales, Ministerio del Medio Ambiente: Madrid, Spain, 2010.

34. Villanueva Aranguren, J.A. *Tercer Inventario Forestal Nacional (1997–2006)*; Ministerio para la Transición Ecológica y el Reto Demográfico: Madrid, Spain, 2001.

35. Shelton, A.O.; Mangel, M. Estimating von Bertalanffy parameters with individual and environmental variations in growth. *J. Biol. Dyn.* **2012**, *6*, 3–30. [CrossRef]

36. Pienaar, L.V.; Turnbull, K.J. The Chapman-Richards Generalization of Von Bertalanffy's Growth Model for Basal Area Growth and Yield in Even- Aged Stands. *For. Sci.* **1973**, *19*, 2–22. [CrossRef]

37. Coble, D.W.; Lee, Y.-J. Use of a generalized sigmoid growth function to predict site index for unmanaged loblol-ly and slash pine plantations in East Texas. In *General Technical Rep. SRS-92*; U.S. Department of Agriculture, Forest Service, Southern Research Station: Asheville, NC, USA, 2006; pp. 291–295.

38. Renner-Martin, K.; Brunner, N.; Kühleitner, M.; Nowak, W.G.; Scheicher, K. On the exponent in the Von Bertalanffy growth model. *PeerJ* **2018**, *6*, e4205. [CrossRef]

39. Vincenzi, S.; Crivelli, A.J.; Munch, S.; Skaug, H.J.; Mangel, M. Trade-offs between accuracy and interpretability in von Bertalanffy random-effects models of growth. *Ecol. Appl.* **2016**, *26*, 1535–1552. [CrossRef]

40. Yuancai, L.; Marques, C.; Macedo, F. Comparison of Schnute's and Bertalanffy-Richards' growth functions. *For. Ecol. Manag.* **1997**, *96*, 283–288. [CrossRef]

41. Strigul, N.; Pristinski, D.; Purves, D.; Dushoff, J.; Pacala, S. Scaling from Trees to Forests: Tractable Macroscopic Equations for Forest Dynamics. *Ecol. Monogr.* **2008**, *78*, 523–545. [CrossRef]

42. Lines, E.R.; Zavala, M.A.; Ruiz-Benito, P.; Coomes, D.A. Capturing juvenile tree dynamics from count data using Approximate Bayesian Computation. *Ecography* **2020**, *43*, 406–418. [CrossRef]

43. Purves, D.W.; Lichstein, J.W.; Strigul, N.; Pacala, S.W. Predicting and understanding forest dynamics using a simple tractable model. *Proc. Natl. Acad. Sci. USA* **2008**, *105*, 17018–17022. [CrossRef]

44. Goldberg, D.E. Competitive ability: Definitions, contingency and correlated traits. *Philos. Trans. R. Soc. B Biol. Sci.* **1996**, *351*, 1377–1385. [CrossRef]

45. Kambach, S.; Allan, E.; Bilodeau-Gauthier, S.; Coomes, D.A.; Haase, J.; Jucker, T.; Kunstler, G.; Müller, S.; Nock, C.; Paquette, A.; et al. How do trees respond to species mixing in experimental compared to observational studies? *Ecol. Evol.* **2019**, *9*, 11254–11265. [CrossRef] [PubMed]

46. Ruiz-Benito, P.; Lines, E.R.; Gómez-Aparicio, L.; Zavala, M.A.; Coomes, D.A. Patterns and Drivers of Tree Mortality in Iberian Forests: Climatic Effects Are Modified by Competition. *PLoS ONE* **2013**, *8*, e56843. [CrossRef] [PubMed]

47. R Core Team. R: A Language and Environment for Statistical Computing. *Vienna, Austria.* 2016. Available online: https://www.R-project.org/ (accessed on 20 April 2021).

48. Soetaert, K.; Petzoldt, T.; Setzer, R.W. Solving Differential Equations in R: Package deSolve. *J. Stat. Softw.* **2010**, *33*, 1–25. [CrossRef]

49. Gómez-Aparicio, L.; García-Valdés, R.; Ruíz-Benito, P.; Zavala, M.A. Disentangling the relative importance of climate, size and competition on tree growth in Iberian forests: Implications for forest management under global change. *Glob. Chang. Biol.* **2011**, *17*, 2400–2414. [CrossRef]

50. Kunstler, G.; Falster, D.S.; Coomes, D.A.; Hui, F.; Kooyman, R.M.; Laughlin, D.C.; Poorter, L.; Vanderwel, M.C.V.C.; Vieilledent, G.; Wright, S.J.; et al. Plant functional traits have globally consistent effects on competition. *Nat. Cell Biol.* **2016**, *529*, 204–207. [CrossRef]

51. Barrio-Anta, M.; Sixto-Blanco, H.; De Viñas, I.C.-R.; Castedo-Dorado, F. Dynamic growth model for I-214 poplar plantations in the northern and central plateaux in Spain. *For. Ecol. Manag.* **2008**, *255*, 1167–1178. [CrossRef]

52. Castedo-Dorado, F.; Diéguez-Aranda, U.; Barrio-Anta, M.; Álvarez-González, J.G. Modelling stand basal area growth for radiata pine plantations in Northwestern Spain using the GADA. *Ann. For. Sci.* **2007**, *64*, 609–619. [CrossRef]

53. Sánchez-Salguero, R.; Camarero, J.J.; Gutiérrez, E.; Rouco, F.G.; Gazol, A.; Sangüesa-Barreda, G.; Andreu-Hayles, L.; Linares, J.C.; Seftigen, K. Assessing forest vulnerability to climate warming using a process-based model of tree growth: Bad prospects for rear-edges. *Glob. Chang. Biol.* **2017**, *23*, 2705–2719. [CrossRef] [PubMed]

54. Rohner, B.; Waldner, P.; Lischke, H.; Ferretti, M.; Thürig, E. Predicting individual-tree growth of central European tree species as a function of site, stand, management, nutrient, and climate effects. *Eur. J. For. Res.* **2018**, *137*, 29–44. [CrossRef]

55. Bravo, F.; Álvarez-González, J.G.; Del Río, M.; Barrio, M.; Bonet, J.A.; Bravo-Oviedo, A.; Calama, R.; Castedo-Dorado, F.; Crecente-Campo, F.; Condés, S.; et al. Growth and yield models in Spain: Historical overview, Contemporary Examples and perspectives. *For. Syst.* **2011**, *20*, 315–328. [CrossRef]

56. Monserud, R.A.; Sterba, H. A basal area increment model for individual trees growing in even- and uneven-aged forest stands in Austria. *For. Ecol. Manag.* **1996**, *80*, 57–80. [CrossRef]

57. Trasobares, A.; Tomé, M.; Miina, J. Growth and yield model for Pinus halepensis Mill. in Catalonia, north-east Spain. *For. Ecol. Manag.* **2004**, *203*, 49–62. [CrossRef]

58. Kunstler, G.; Guyennon, A.; Ratcliffe, S.; Rüger, N.; Ruiz-Benito, P.; Childs, D.Z.; Dahlgren, J.; Lehtonen, A.; Thuiller, W.; Wirth, C.; et al. Demographic performance of European tree species at their hot and cold climatic edges. *J. Ecol.* **2021**, *109*, 1041–1054. [CrossRef]

59. García-Callejas, D.; Molowny-Horas, R.; Retana, J. Projecting the distribution and abundance of Mediterranean tree species under climate change: A demographic approach. *J. Plant Ecol.* **2016**, *10*, 731–743. [CrossRef]

60. Vizcaíno-Palomar, N.; Gómez-Aparicio, L.; Pavón-García, J.; Bartolomé-Esteban, C.; Álvarez-Jiménez, J.; Zavala, M.A. Main biotic drivers of tree growth in a developing Juniperus thurifera stand in central Spain. *Eur. J. For. Res.* **2014**, *133*, 1109–1119. [CrossRef]

61. Astigarraga, J.; Andivia, E.; Zavala, M.A.; Gazol, A.; Cruz-Alonso, V.; Vicente-Serrano, S.M.; Ruiz-Benito, P. Evidence of non-stationary relationships between climate and forest responses: Increased sensitivity to climate change in Iberian forests. *Glob. Chang. Biol.* **2020**, *26*, 5063–5076. [CrossRef] [PubMed]

62. Ruiz-Benito, P.; Ratcliffe, S.; Jump, A.S.; Gómez-Aparicio, L.; Madrigal-González, J.; Wirth, C.; Kändler, G.; Lehtonen, A.; Dahlgren, J.; Kattge, J.; et al. Functional diversity underlies demographic responses to environmental variation in European forests. *Glob. Ecol. Biogeogr.* **2017**, *26*, 128–141. [CrossRef]

63. Melesse, S.F.; Zewotir, T. Additive mixed models to study the effect of tree age and climatic factors on stem radial growth of Eucalyptus trees. *J. For. Res.* **2020**, *31*, 463–473. [CrossRef]